Switching selectivity between Pb^{2+} and Hg^{2+} ions through variation of substituents at xanthene end; 'turn-on' signalling responses by FRET modulation

Biswonath Biswal and Bamaprasad Bag*

Colloids and Materials Chemistry Department, Academy of Scientific and Innovative Research, CSIR-Institute of Minerals and Materials Technology, P.O.: R.R.L., Bhubaneswar-751 013, Odisha, India. Fax: (+) 91 674 258 1637; Tel: (+ 91) 674 237 9254, Email: *bpbag@immt.res.in*

Electronic Supplementary Information

Materials and methods:

All the reagent grade chemicals were used as received and without purification unless mentioned otherwise. All the solvents were freshly distilled prior to use for fluorescence measurements by following the literature procedures and all the reactions were carried out under a N_2 atmosphere. Chromatographic separations were done by column chromatography using 100–200mesh silica gel or neutral alumina. The compounds were characterized by elemental analysis, ^{1}H-NMR, ^{13}C-NMR and mass(ESI) spectroscopy. ^{1}H-NMR and ^{13}C-NMR spectra were recorded on a JEOL JNM-AL400FTV 4.0 AL 400(400MHz) instrument in $CDCl_3$ with Me_4Si as the internal standard. Electrospray mass spectral data were recorded on a MICROMASS QUATTROII Triple quadruple mass spectrometer. The dissolved samples of the compounds in suitable solvents were introduced into the ESI source through a syringe pump at the rate of 5 mL min^{-1}, ESI capillary was set at 3.5kV with 40V cone voltage and the spectra were recorded at 6s scans. Melting points were determined with a melting point apparatus by BIBBY Scientific limited, India and were uncorrected. Elemental analyses were done in an Elementar Vario ELIII Carlo Erba1108 elemental analyzer. The single crystal data was collected using Bruker-Kappa Apex II X-ray diffractometer. UV–visible spectra were recorded on a Perkin Elmer Lambda 650 UV/VIS spectrophotometer at 298K in 10^{-5}M concentration. Steady-state fluorescence spectra were obtained with a Fluoromax 4P spectrofluorometer at 298 K with very dilute solutions (1-0.01μM) of the samples to avoid auto quenching. As required in case to case basis, fluorescence quantum yields were determined by comparing the corrected spectrum with that of either rhodamine G ($\phi_F = 0.95$) or anthracene($\phi_F = 0.297$) in EtOH by taking area under total emission using following eqn.,

$$\phi_S = \phi_R \left(\frac{F_S A_R}{F_R A_S}\right) \cdot \left(\frac{\eta_S}{\eta_R}\right)^2 \qquad \ldots\ldots \qquad \ldots\ldots \text{ eqn. S1}$$

where ϕ_S and ϕ_R are the radiative quantum yields, F_S and F_R are the area under the fluorescence spectra, A_S and A_R are the absorbance (at the excited wavelength) of the respective sample and the reference; η_S and η_R are the refractive indices of the solvent used for the sample and the reference. The quantum yield of Rhodamine G was measured using quinine sulfate in 1N H_2SO_4 as reference excited at (λ_{ex}) 350 nm. The standard quantum yield value thus obtained was used for the calculation of the quantum yield of the samples.

The complex stability constants[22] (Ks) of the probes with various metal ions and their detection limit[26] were determined following known methods. The Pb^{2+}-**L₂** interaction in incubated *E. Coli* were probed using a Nikon 80i (Nikon Inc., Japan) fluorescence

microscope. Deionised water was used for all experiments, no buffer were used to avoid cross contamination unless otherwise specified for pH studies.

The singlet-singlet excitation energy transfer (η_{EET}) efficiency between anthracene(D_{An}) donor and rhodamine(A_{Rh}) acceptor was evaluated from steady-state fluorescence data following the equation (eqn. S2).

$$\eta_{EET} = 1 - F_{DA}/ F_D \dots \dots \dots \text{Eqn. S2.}$$

where F_{DA} and F_D are the fluorescence intensities of donor (D_{An}) in presence and absence of the acceptor respectively.

Forster's critical distance (R_0), the distance at which 50% energy transfer takes place in between donor and acceptor pair was determined following equation (eqn. S3)

$$R_0 = 0.2108 \times \left[\kappa^2 \times \phi_D \times n_R^{-4} \times J(\lambda) \right]^{1/6} \dots \dots \dots \text{Eqn. S3}$$

where κ^2 is the orientation factor between emission and absorption dipoles which depends on their relative orientation, ϕ_D is quantum yield of donor in absence of receptor, n_R is refractive index of medium, and $J(\lambda)$ is overlap integral of fluorescence emission spectrum of the donor and absorption spectrum of the acceptor which is expressed as shown in eqn. S4.

$$J(\lambda) = \int_0^\infty F_D(\lambda) \times \in_A(\lambda) \times (\lambda)^4 \times d\lambda \dots \dots \dots \text{Eqn. S4}$$

where F_D is the normalized fluorescence of the donor, ε_A is the molar extinction coefficient of the acceptor (in $dm^3\ mol^{-1}\ cm^{-1}$) and λ is the wavelength in nm.

Determination of association constant (K_a):

The association constant (K_a) of the complex were determined from the change in absorbance or fluorescence resulted from titration of dilute solutions ($\sim 10^{-5}$-10^{-7} M) of probes against metal ion solution following Benesi-Hildebrand method for a complexation of 1:1 (ligand: metal) stoichiometry as depicted in eqn.S5, *i. e.*

$$1/(X-X_0) = 1/\{K_a(X_{max}-X_0)[M(II)]\} + 1/(X_{max}-X_0) \quad \dots \dots \dots \text{Eqn. S5}$$

where X_0 is absorbance or fluorescence of **probe** at a particular wavelength, X is absorbance or fluorescence intensity obtained with added [M(II)], X_{max} is absorbance or fluorescence obtained with excess amount of metal ion added and [M(II)] is concentration of metal ion added. The double reciprocal plot of absorption or fluorescence spectral change $\{1/(X-X_0)\}$ as a function of added metal ion concentration ($1/[M^{2+}]$) results in a linear regression and its slope determines K_a.
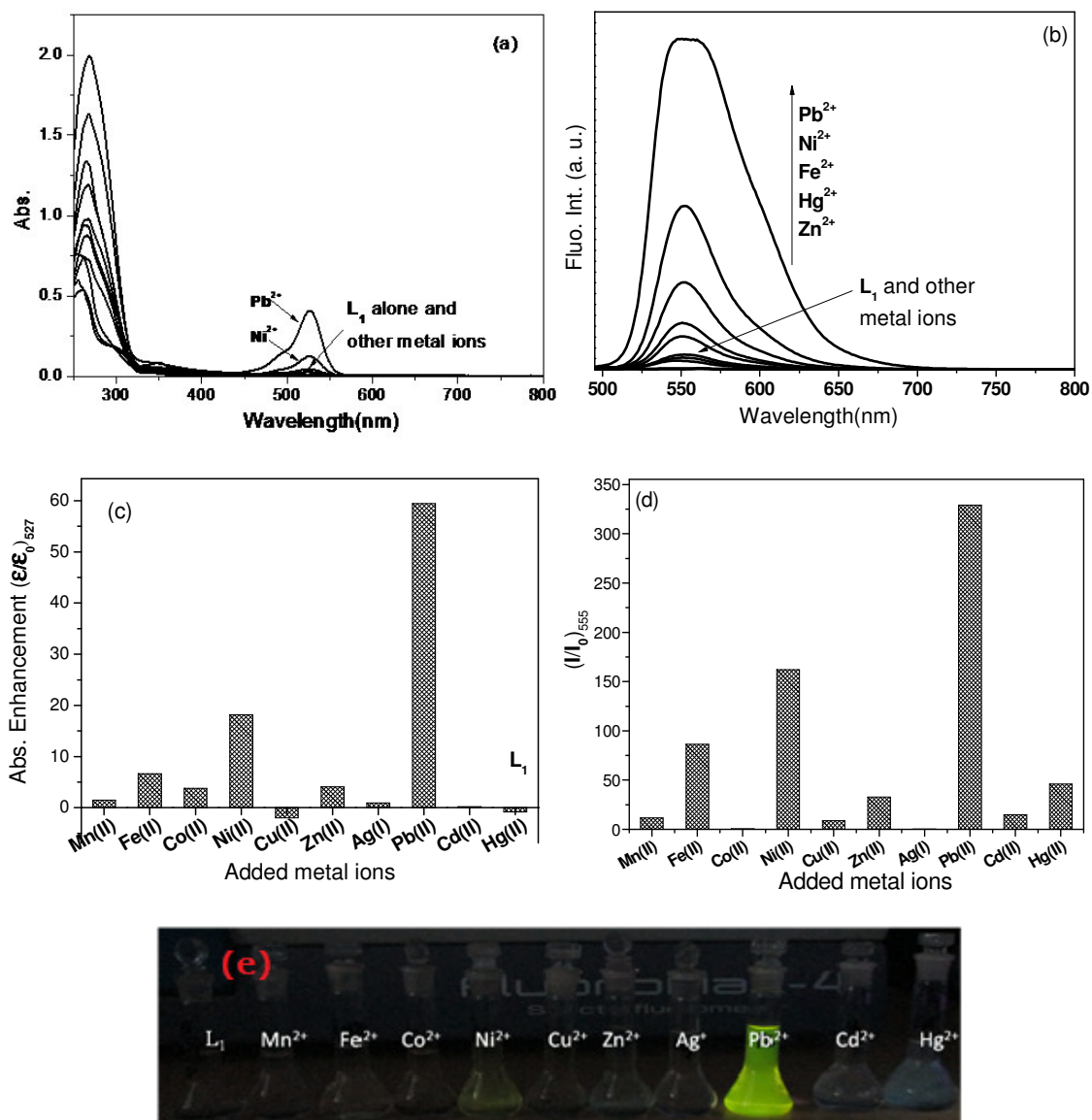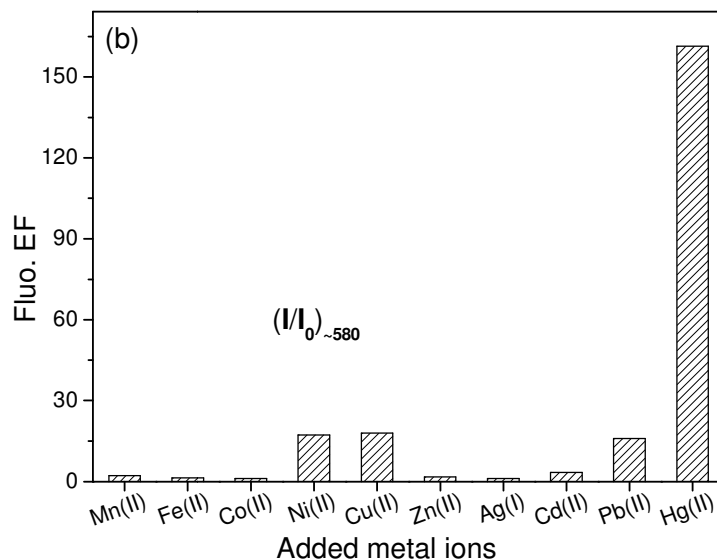
Fig. S1: (a)Absorption and (b)fluorescence spectra of **L₁** in absence and presence of various metal ions in CH₃CN-H₂O(9.5 : 0.5 v/v) and the corresponding metal ion induced absorption (c) and fluorescence (d) enhancements. (e) Photograph depicting colour of the solution after addition of metal ions under 350nm illumination. [**L₁**]=10μM (abs), 1μM (em), λ_{ex}= 480 nm, em. and ex. bp = 5nm, RT. [**M$^{+1/+2}$**] = 50μM(abs), 10μM (em).
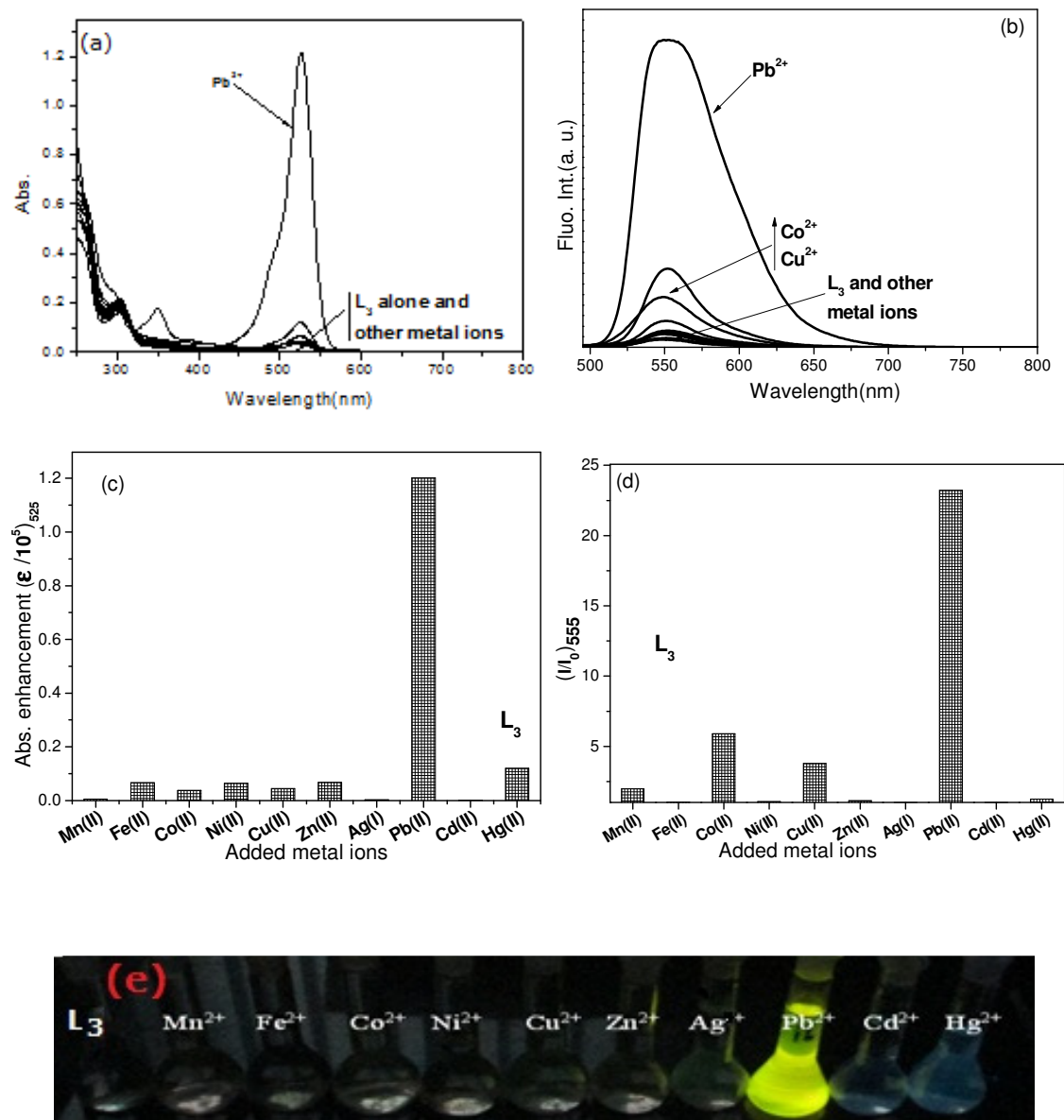
Fig. S2. (a)Absorption and (b)fluorescence spectra of **L₃** in absence and presence of various metal ions in CH_3CN-H_2O(9.5 : 0.5 v/v) and the corresponding metal ion induced absorption (c) and fluorescence (d) enhancements. (e) Photograph depicting colour of the solution after addition of metal ions under 350nm illumination. [**L₃**]=10μM (abs), 1μM (em), λ_{ex}= 480 nm, em. and ex. bp = 5nm, RT. [**M$^{+1/+2}$**] = 50μM(abs), 10μM (em).
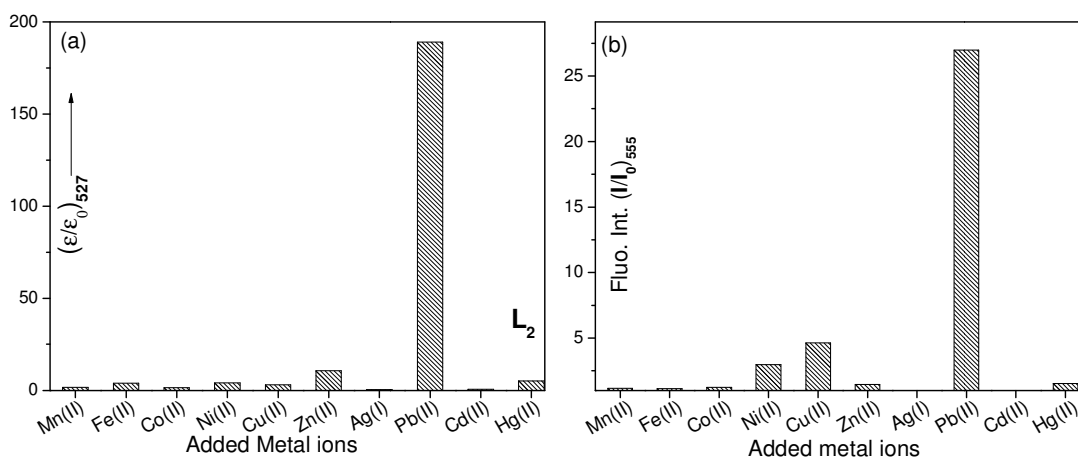
Fig. S3. (a) Absorption(A_{527}) and (b) fluorescence(I_{555}) spectral enhancements of **L₂** in presence of various metal ions in CH_3CN-H_2O(9.5 : 0.5 v/v). [**L₂**]=10μM (abs), 1μM (em), λ_{ex}= 350 nm, em. and ex. bp = 5nm, RT. [$M^{+1/+2}$] = 50μM(abs), 10μM (em).

Fig. S4. (a) Photograph depicting colour of the solution of **L₄** in CH_3CN-H_2O(9.5 : 0.5 v/v) after addition of metal ions under 350nm illumination, (b) corresponding metal ion induced fluorescence enhancements. [**L₄**]= 1μM, λ_{ex}= 500 nm, em. and ex. bp = 5nm, RT, [$M^{+1/+2}$] = 10μM (em), monitored at 580 nm.
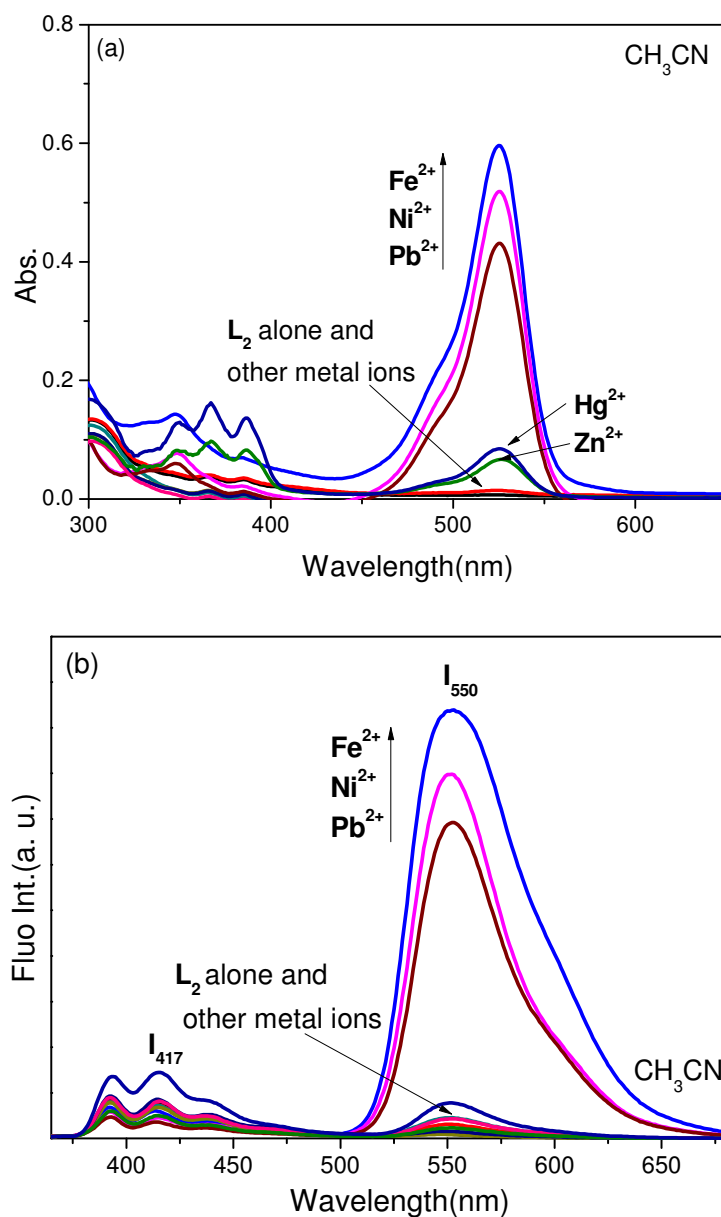
Fig. S5. (a) Absorption and (b) emission spectral pattern of **L₂** in absence and presence of various metal ions in **dry acetonitrile** medium [**L₂**]=10μM (abs), 1μM (em), λ_{ex}= 350nm, em. and ex. bp = 5nm, RT. [$M^{+1/+2}$] = 50μM(abs), 10μM (em).
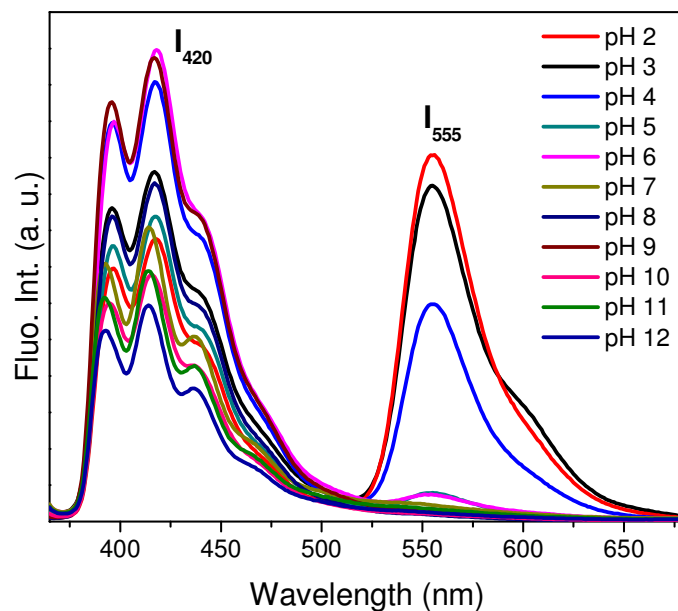
Fig. S6. Emission spectral pattern of **L₂** alone in various pH. [**L₂**]= 1μM, λ_{ex}= 350nm, em. and ex. bp = 5nm, RT.
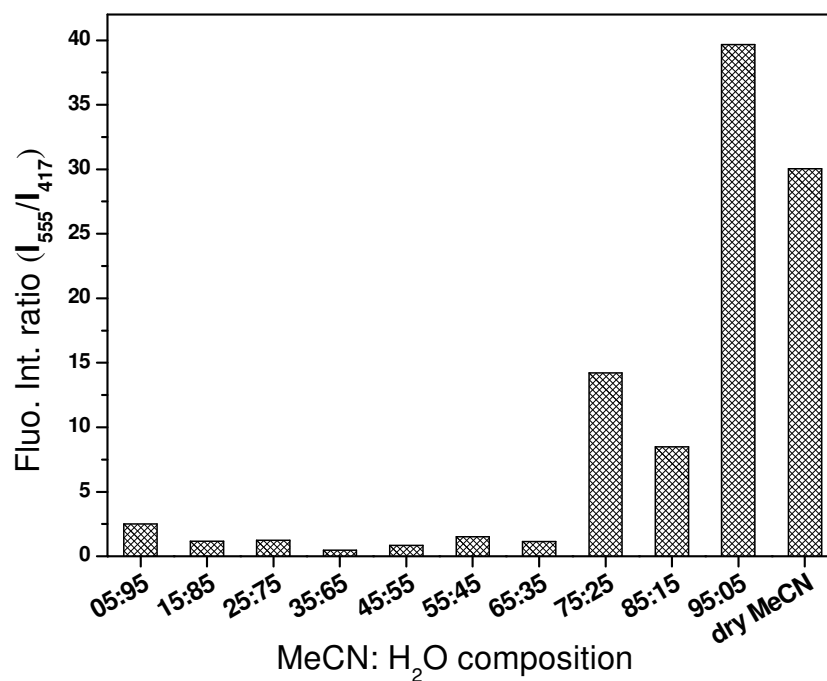
Fig. S7. Fluorescence spectral ratio (I_{555}/I_{417}) of **L₂** in presence of Pb^{2+} in various binary composition of CH_3CN and H_2O solvent mixture. [**L₂**]= 1μM, [Pb^{2+}] =10μM, λ_{ex}= 350nm, em. and ex. bp = 5nm, RT.
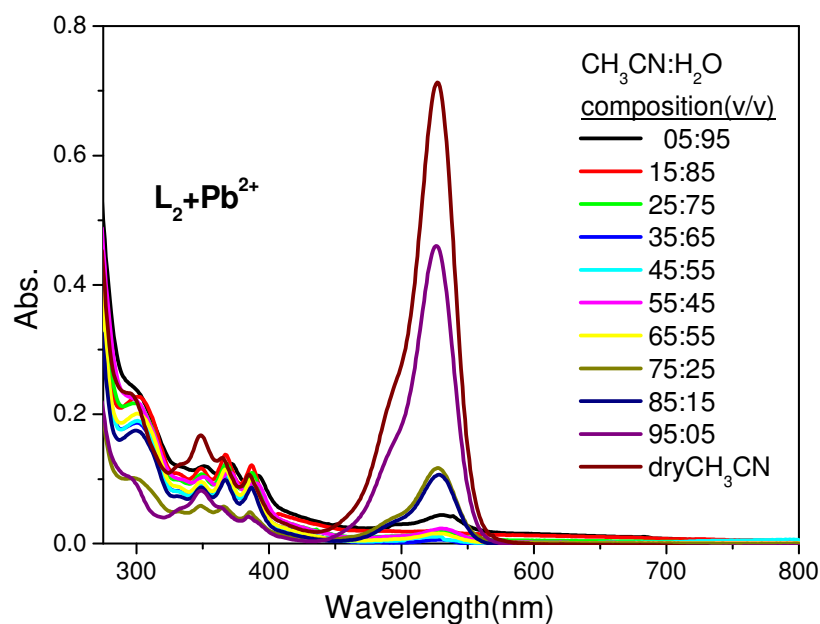
Fig. S8. Absorption spectral pattern of L_2 in presence of Pb^{2+} in different binary composition of CH_3CN and H_2O as solvent. $[L_2]$= 10μM, $[Pb^{2+}]$ =50μM.
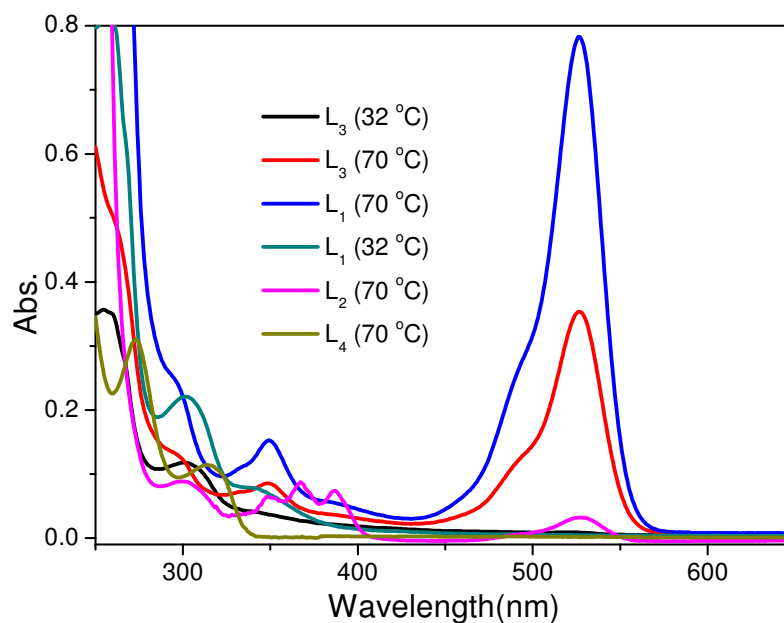
Fig. S9. Absorption spectra of all probes (L_1, L_2, L_3 and L_4) alone in ethanol measured at two different temperatures (32°C and 70°C) showing their stability.
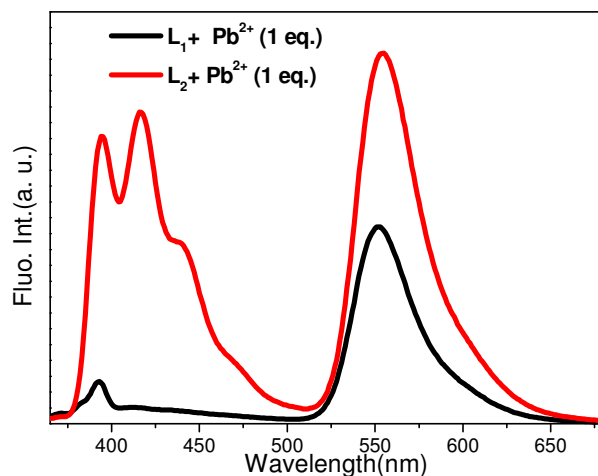
Fig. S10. Comparison of fluorescence spectra of L_1 and L_2 in presence of Pb^{2+} (1 eq.) in MeCN-H_2O(9.5:0.5(v/v) medium when excited at 350nm. $[L_1]= [L_2]= [Pb^{2+}] = 1\mu M$, $\lambda_{ex}= 350$nm, em. and ex. bp = 5nm, RT, the spectra were recorded after 1h of mixing.
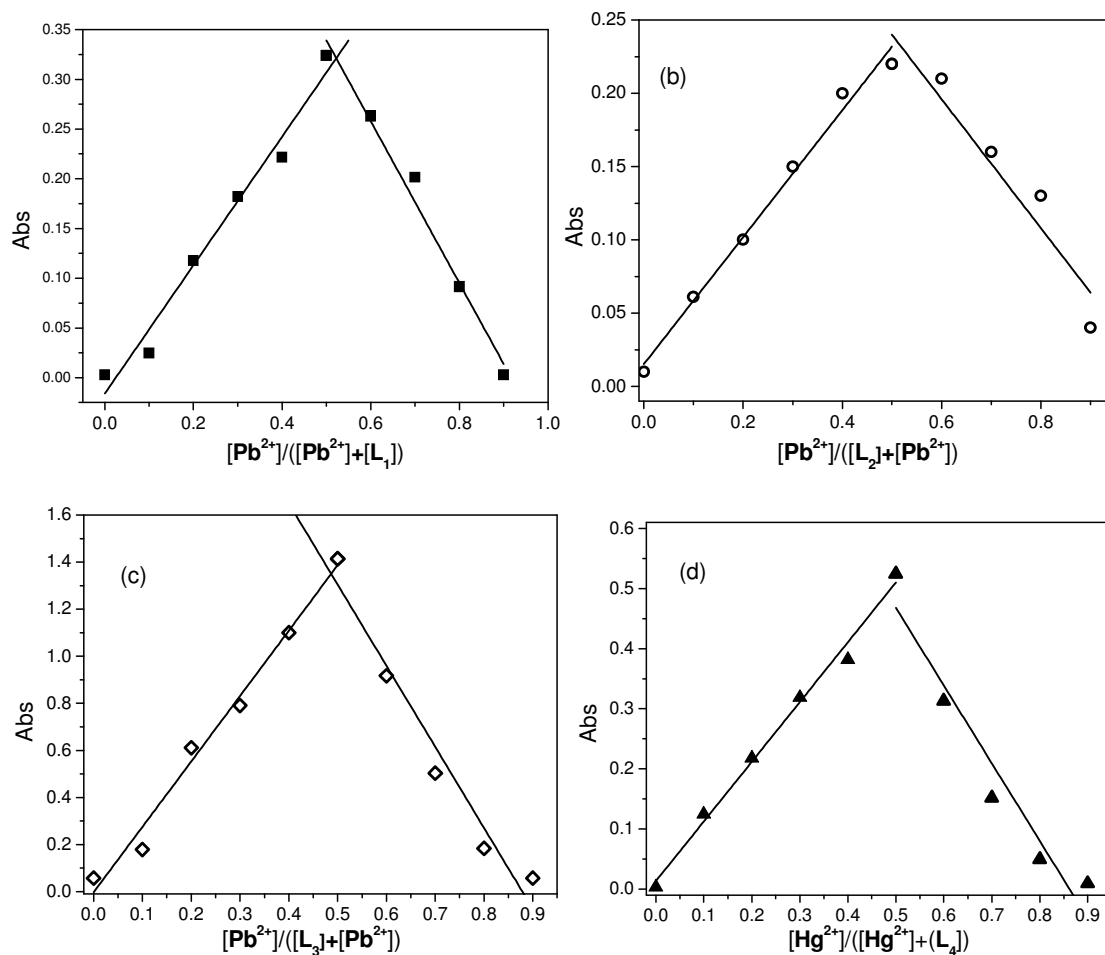
Fig. S11. Job's plot(A_{Rh}) of L_1(a), L_2(b), and L_3(c) with mole fractions of added Pb^{2+} and L_4(d) with that of added Hg^{2+} in MeCN-H_2O(9.5:0.5 v/v) for determination of complexation stoichiometry, which was found to be in 1:1 (L:M) ratio.
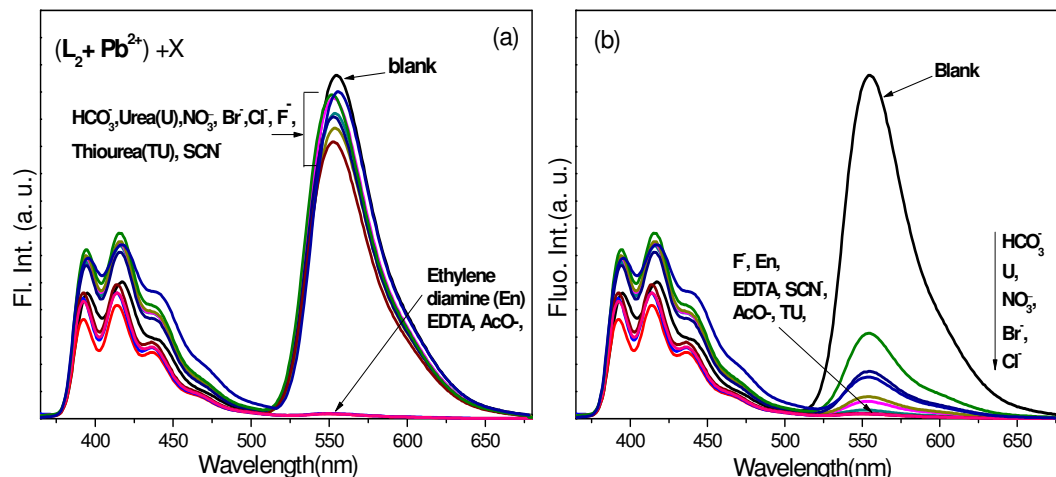
Fig. S12. Fluorescence spectra of L_2-Pb^{2+} in absence and presence of anions and chelating reagents in CH_3CN-H_2O (9.5: 0.5 v/v), λ_{ex}= 350nm, em and ex bp = 5nm, RT, $[L_2]$ =1µM, $[Pb^{2+}]$ = 5µM, [anions] = 10µM. The spectra were recorded (a) immediate and (b) after 12h of addition of anions.
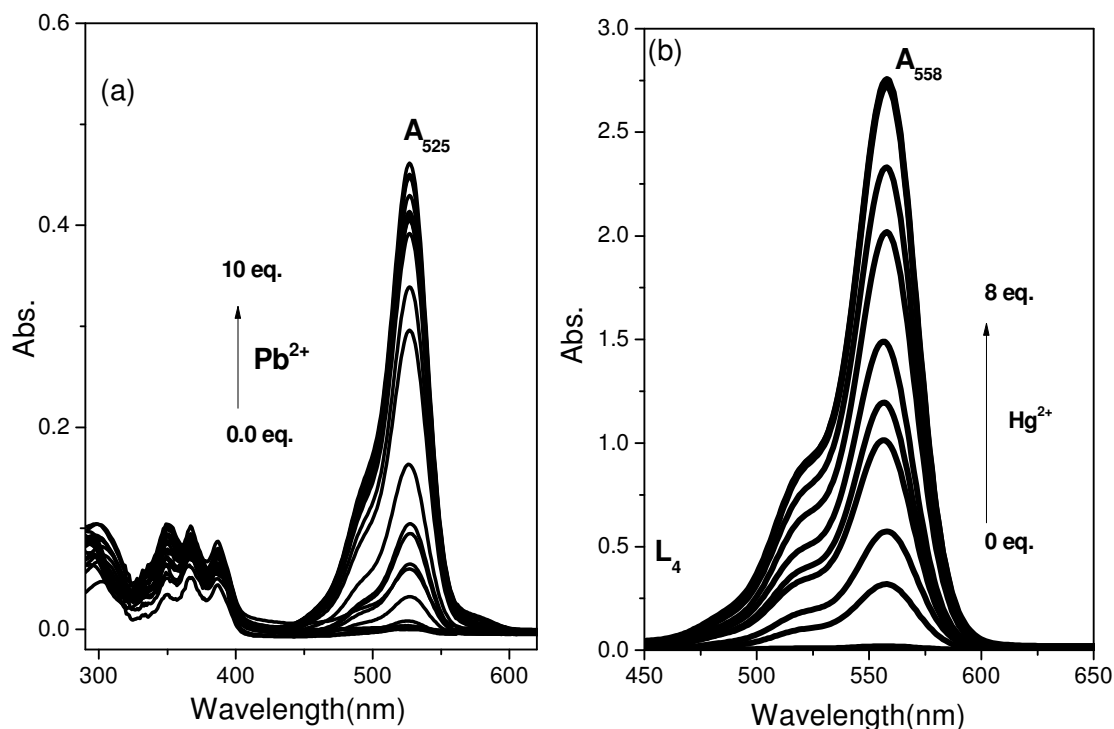
Fig. S13. Absorption spectral pattern of (a) L_2 as a function of added Pb^{2+} and (b) L_4 as a function of added Hg^{2+} ions. The titration profile has been used to determine respective association constants of complexation. $[L_2]$ = 1×10^{-5}M, $[L_4]$ = 1×10^{-4}M, CH_3CN-H_2O (9.5: 0.5 v/v).
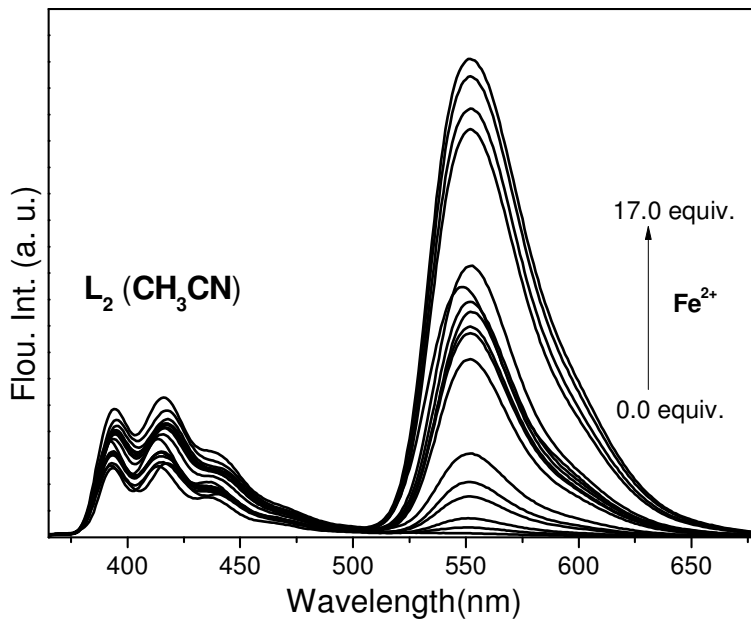
Fig. S14. Absorption spectral pattern of (a) L_2(1μM) as a function of added Fe^{2+} ion in **dry CH$_3$CN** as solvent. λ_{ex}= 350nm, em and ex bp = 5nm, RT.

Eqn.	y = a + b*x		
Adj R-Sq.	0.99349		
		Value	Std. Error
F	Intercept	-1.2056E-7	2.8549E-8
F	Slope	8.81579E-13	1.84189E-14
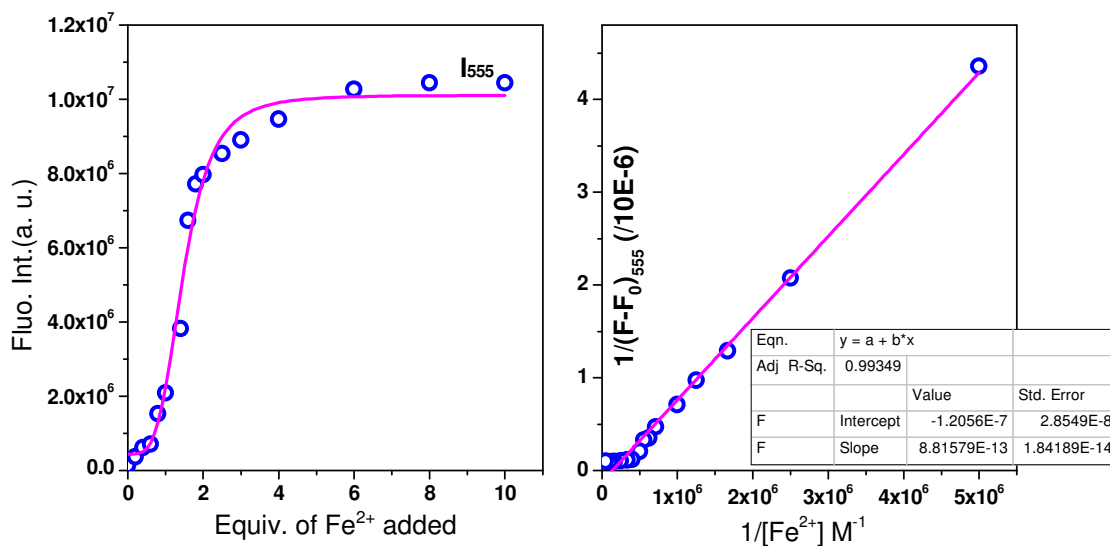
Fig. S15. (a) Plot of fluorescence intensity $(F-F_0)_{555}$ of L_2 (1μM) as a function of equivalents of added Fe^{2+} ions in **dry CH$_3$CN**. (b) Double reciprocal plot of change in fluorescence against concentration Fe^{2+} ions added for determination of complex association constant(Ka).
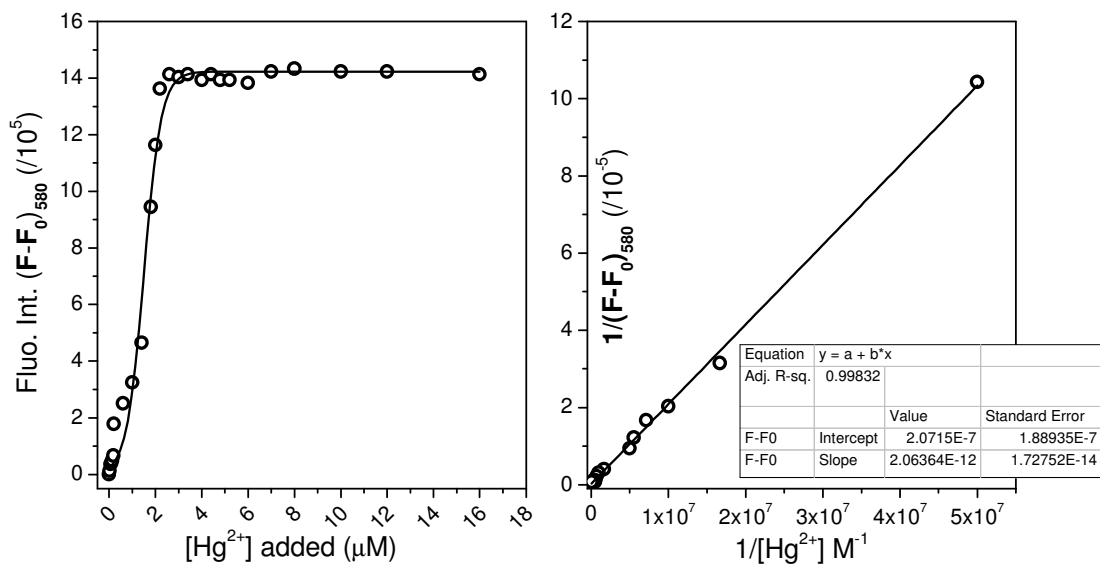
Fig. S16. (a) Plot of fluorescence intensity $(F-F_0)_{580}$ of **L4** (1µM) as a function of concentration of added Hg^{2+} ions in CH_3CN-H_2O (9.5: 0.5 v/v). (b) Double reciprocal plot of change in fluorescence against concentration Hg^{2+} ions added, reciprocal of the slope of linear regression determines K_a.
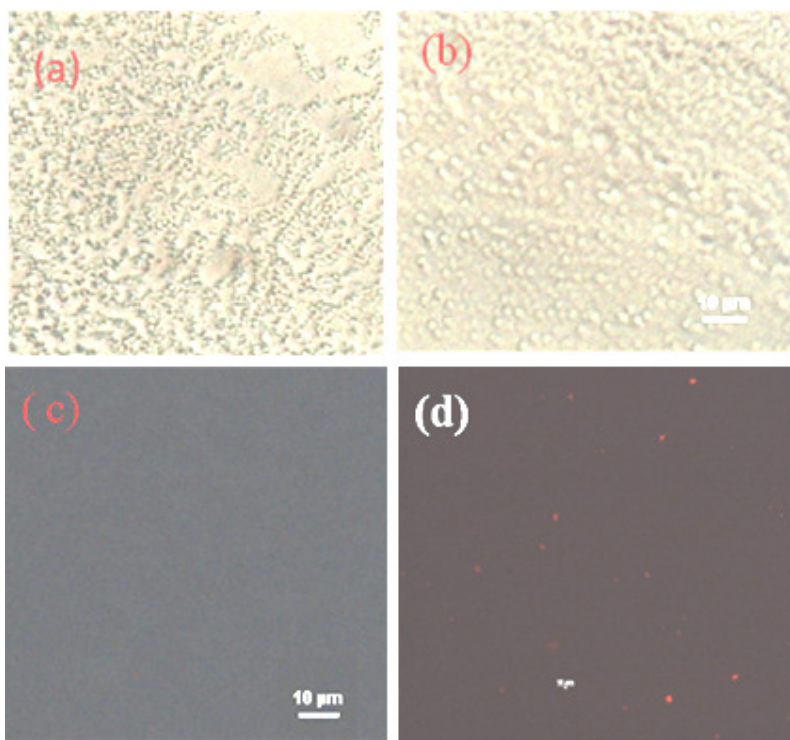
Fig. S17. Bright field images of *E. Coli* alone (a) and when incubated with **L2**(b). Their fluorescence image on incubation with **L2** before(c) and after(d) addition of Pb^{2+} ion, $\lambda_{ex} \approx$ 350nm.
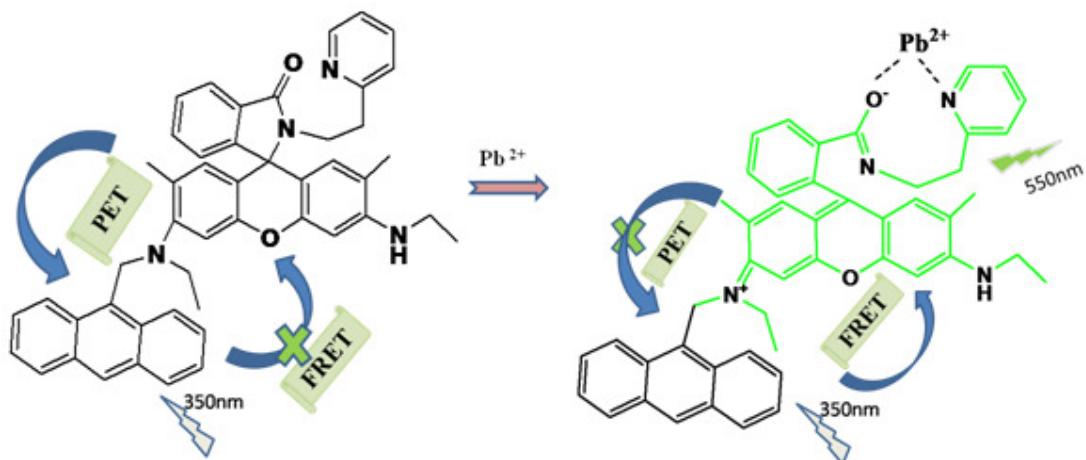
Fig. S18. Pictorial representation of modulation various operation processes in **L₂** in absence and presence of Pb^{2+} showing signal mechanism.
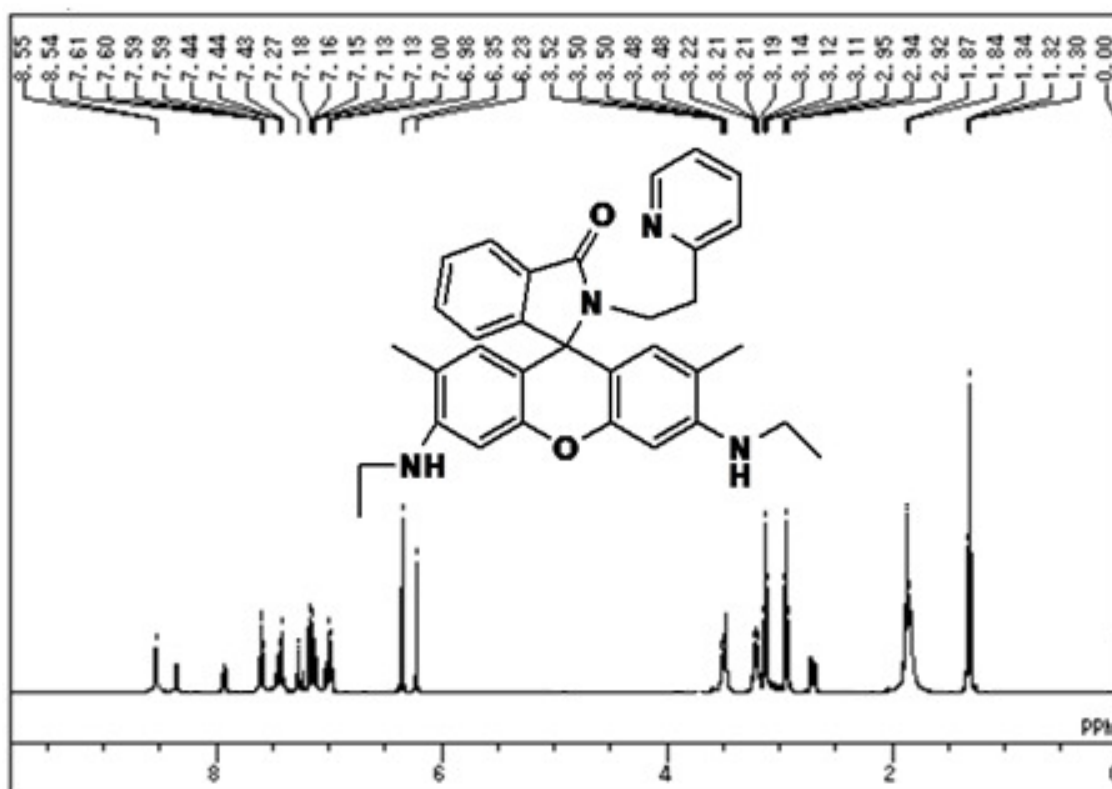
Fig. S19. ¹H-NMR spectrum of **L₁** in CDCl₃
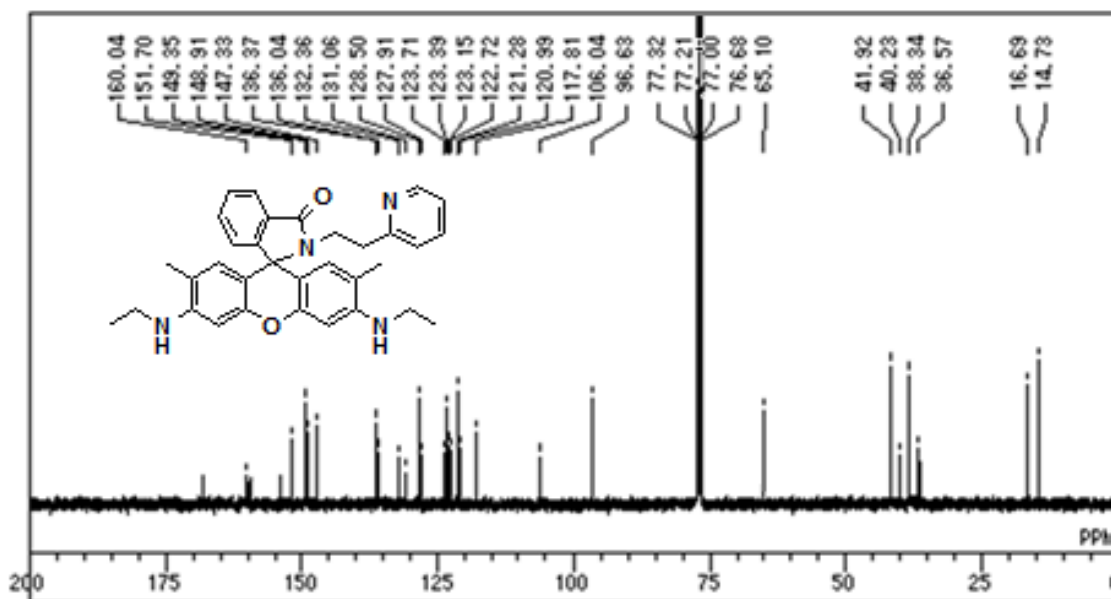
Fig. S20. ^{13}C-NMR spectrum of **L$_1$** in CDCl$_3$
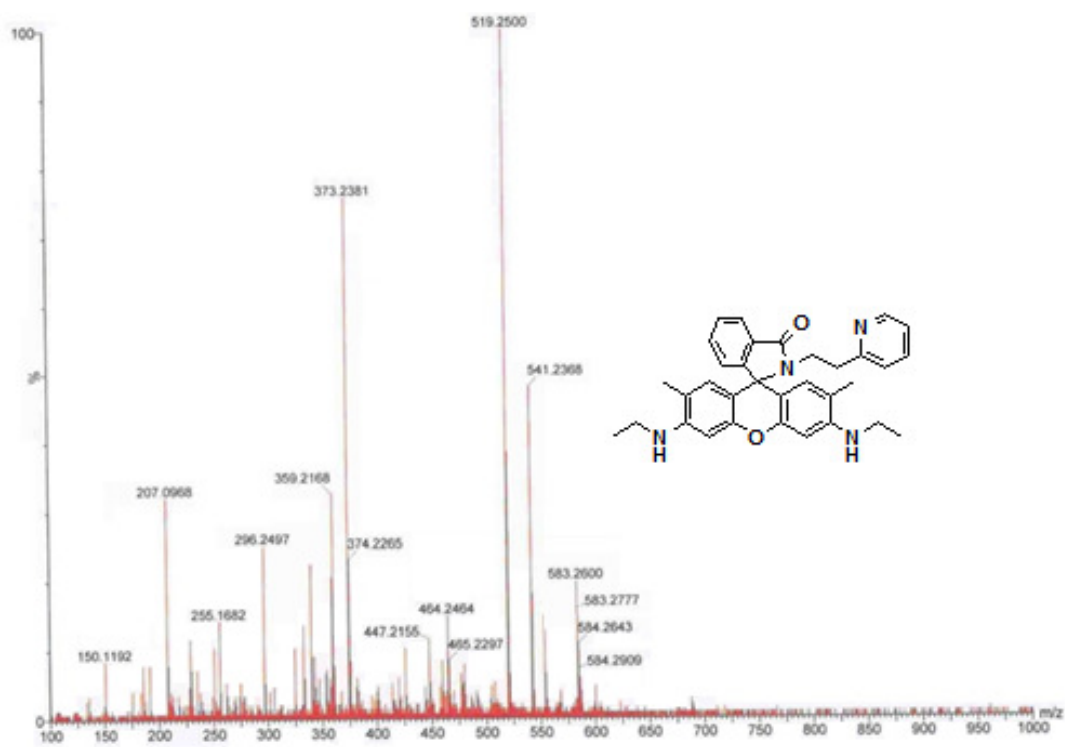
Fig. S21. ESI-MS spectrum of **L$_1$**
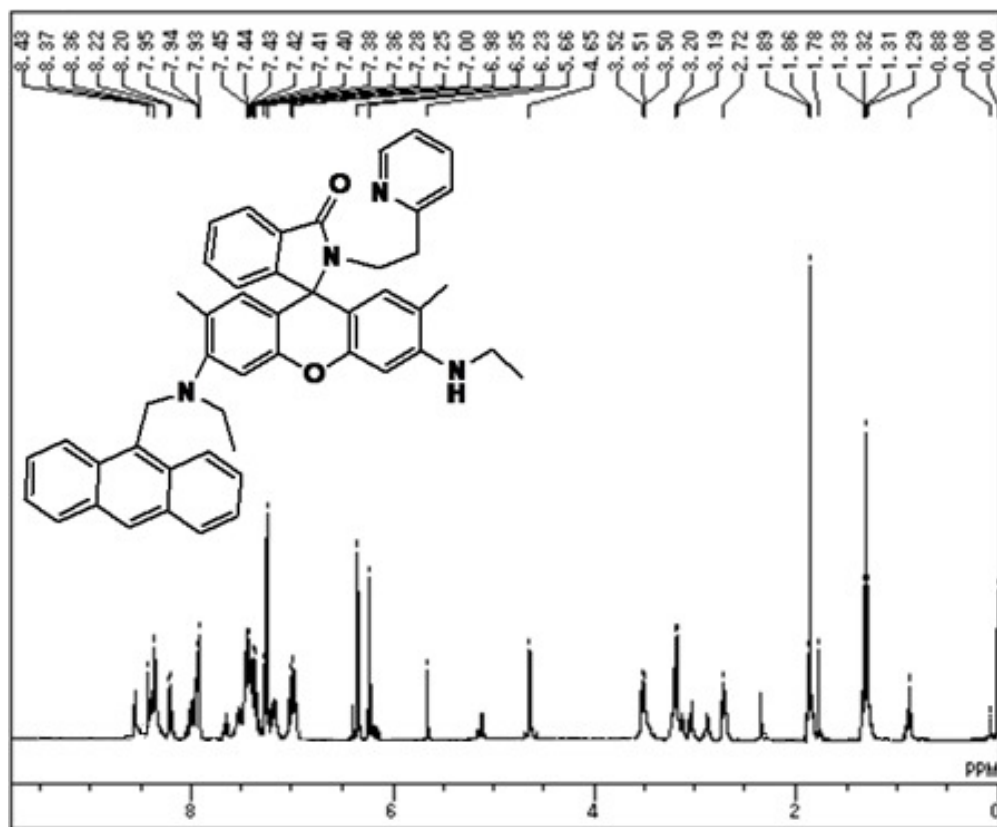
Fig. S22. ^{1}H-NMR spectrum of **L₂** in CDCl₃
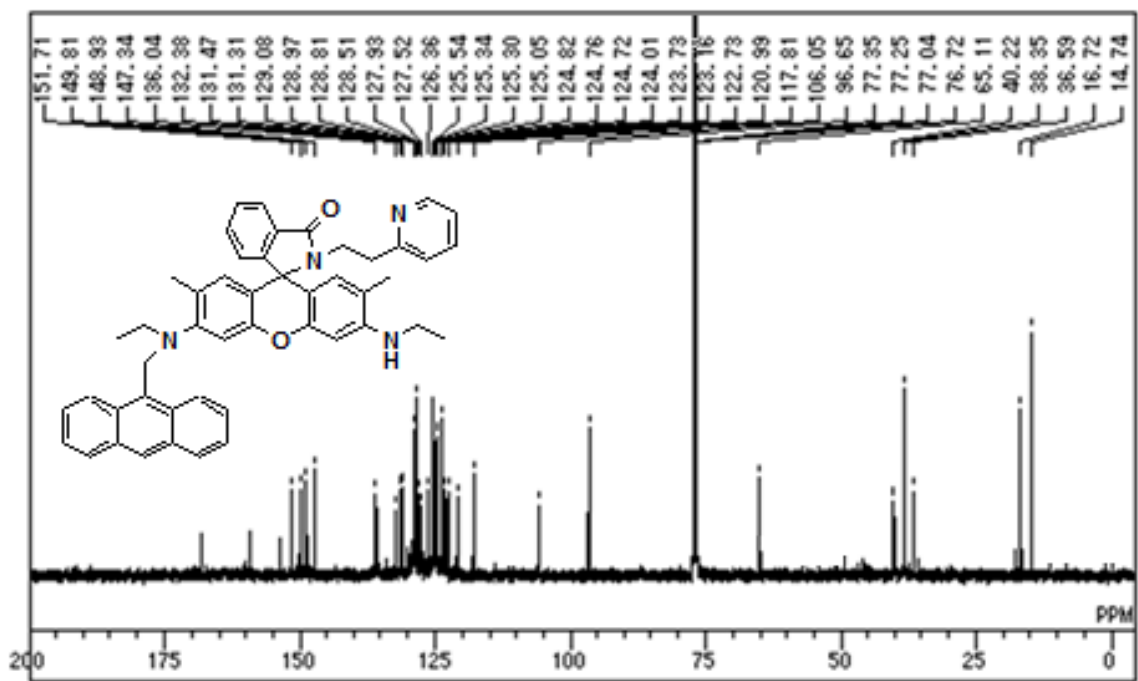
Fig. S23. ^{13}C-NMR spectrum of **L₂** in CDCl₃
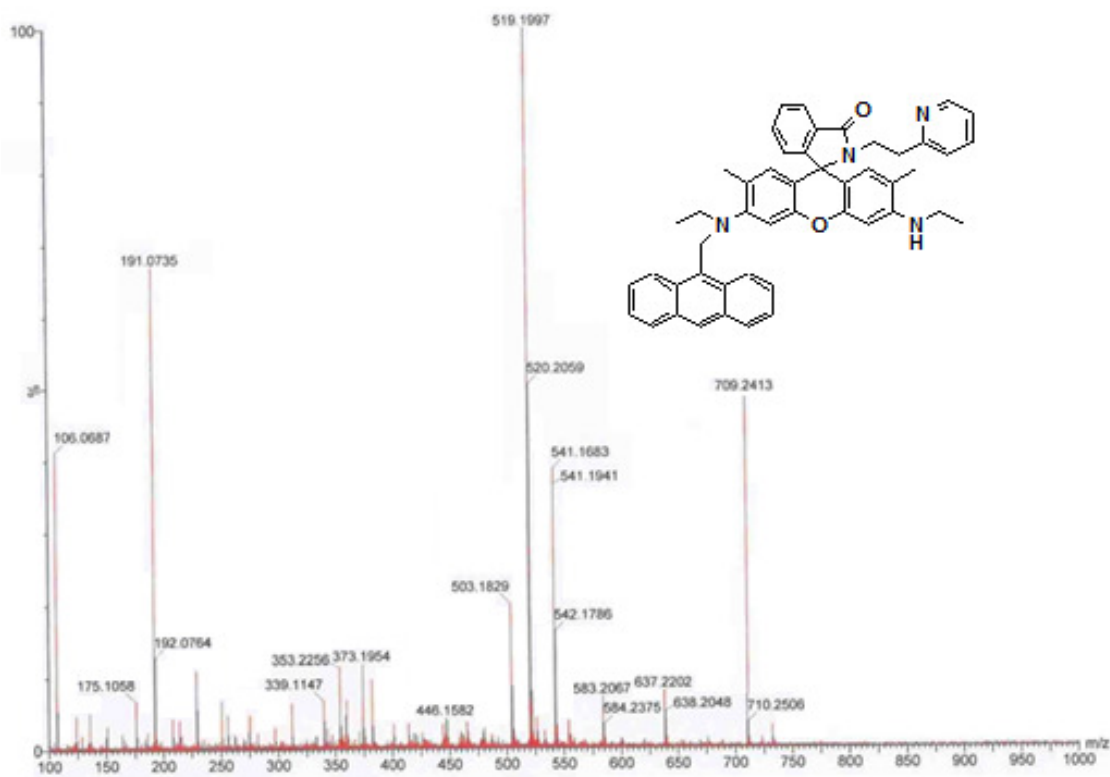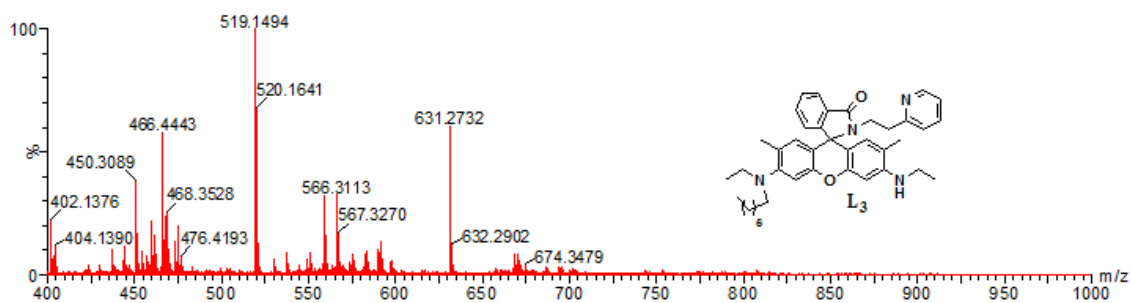
Fig. S24. ESI-MS spectrum of **L₂**
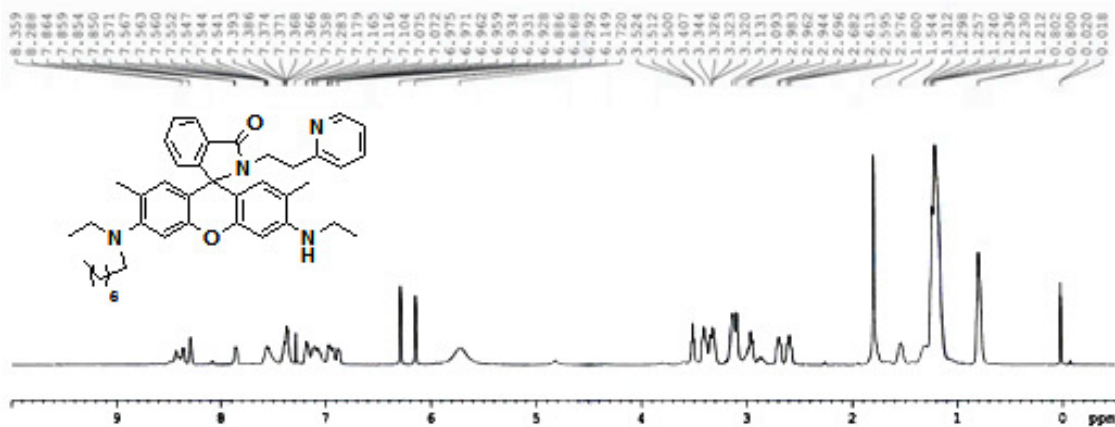
Fig. S25. ^{1}H-NMR spectrum of **L₃** in CDCl₃
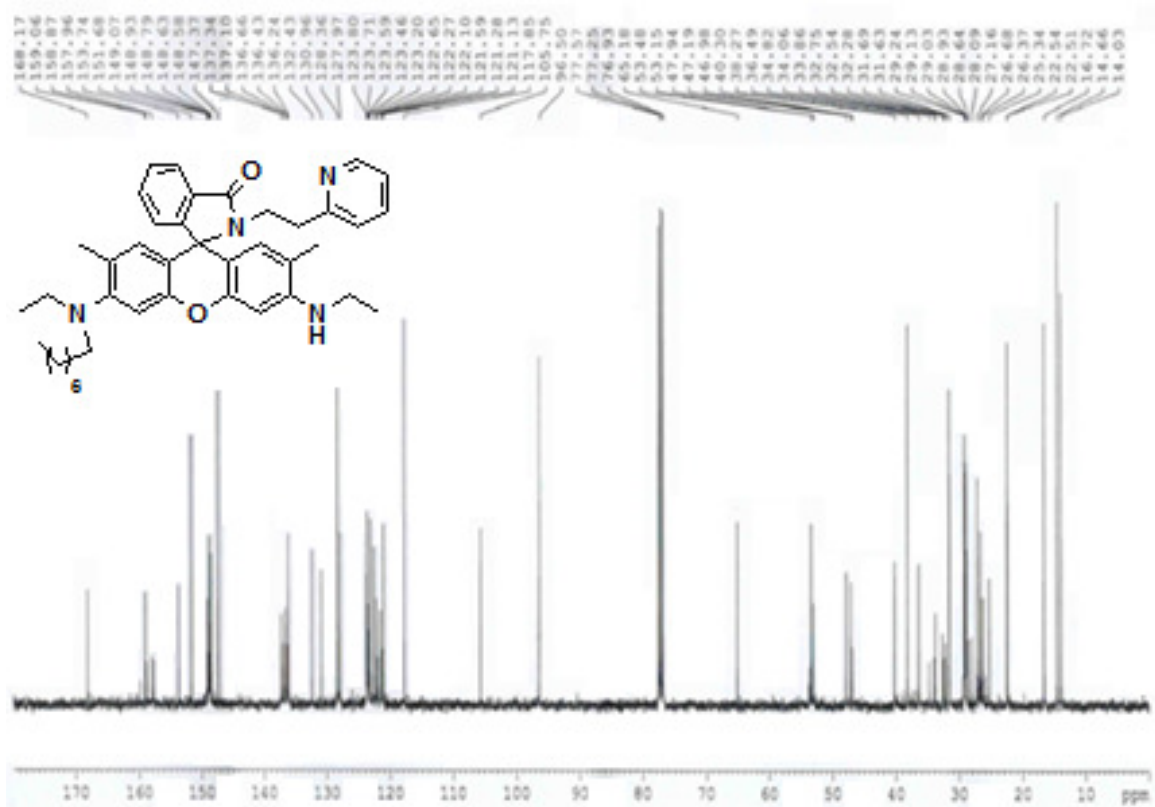
Fig. S26. ^{13}C-NMR spectrum of **L$_3$** in CDCl$_3$

Fig. S27. ESI-MS spectrum of **L$_3$**

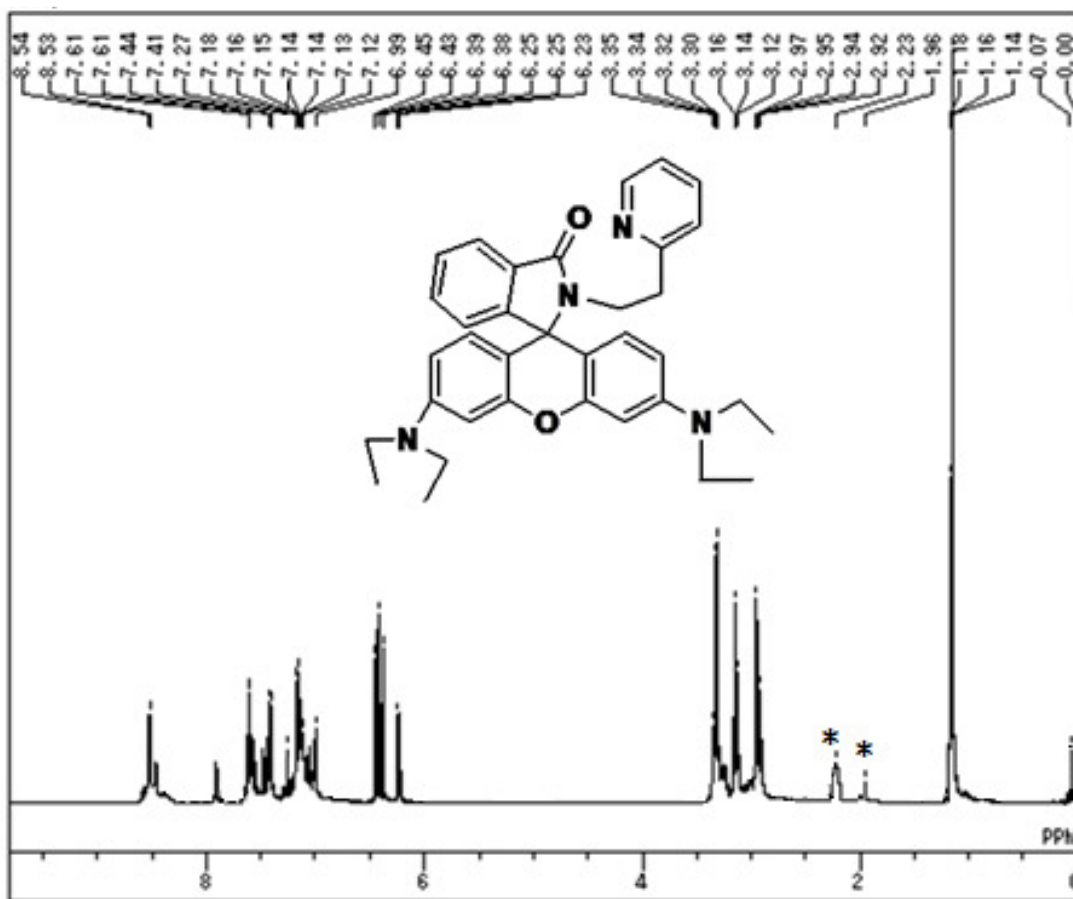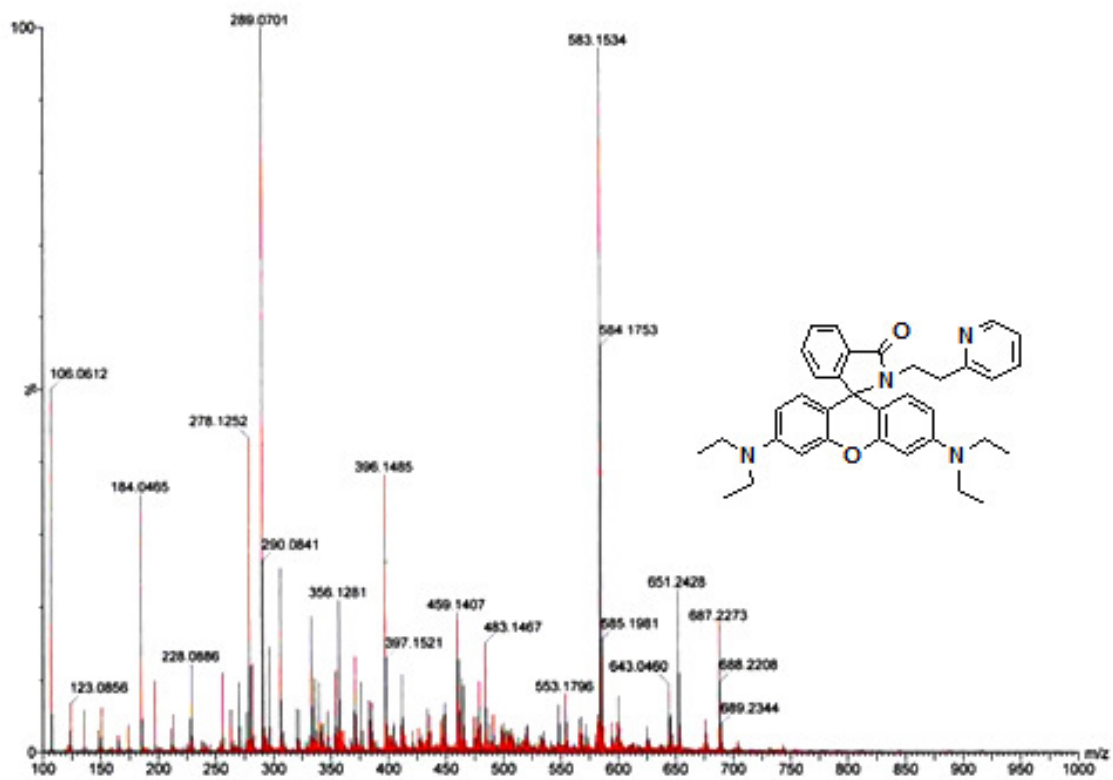**Fig. S28**. ^{1}H-NMR spectrum of **L$_4$** in CDCl$_3$
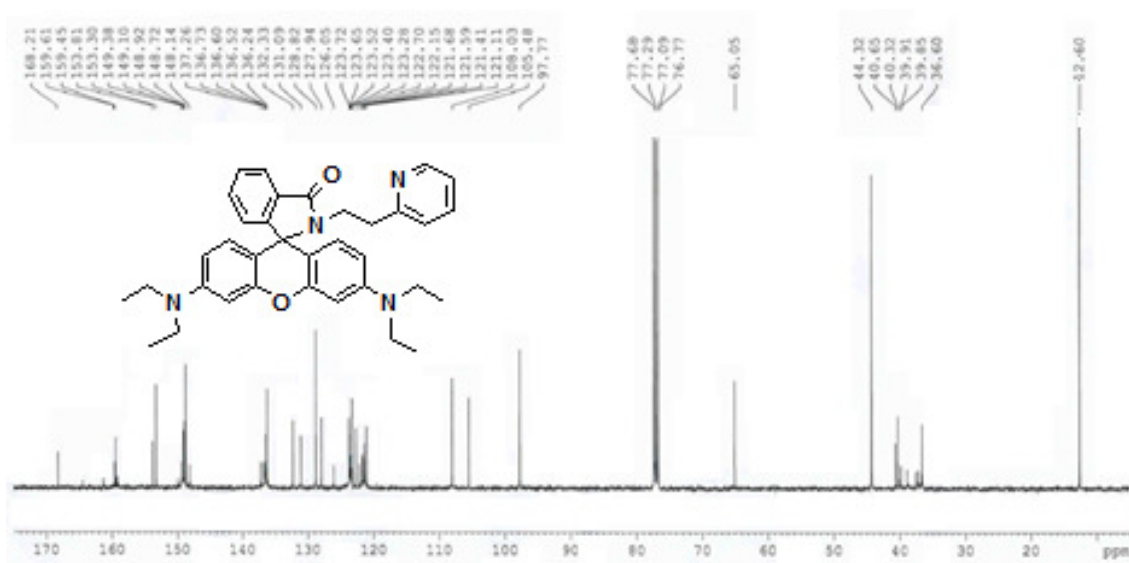
Fig. S29. ^{13}C-NMR spectrum of **L$_4$** in CDCl$_3$

Fig. S30. ESI-MS spectrum of **L₄**